Article

Spectroscopic and Computational Study of the Protonation Equilibria of Amino-Substituted benzo[*b*]thieno[2,3-*b*]pyrido[1,2-*a*]benzimidazoles as Novel pH-Sensing Materials

Nataša Perin [1], Darko Babić [2], Petar Kassal [3], Ana Čikoš [4], Marijana Hranjec [1,*] and Robert Vianello [5,*]

[1] Department of Organic Chemistry, Faculty of Chemical Engineering and Technology, University of Zagreb, Marulićev trg 19, 10000 Zagreb, Croatia; nperin@fkit.hr
[2] Group for Theoretical Chemistry, Ruđer Bošković Institute, Bijenička cesta 54, 10000 Zagreb, Croatia; darko.babic@irb.hr
[3] Department of General and Inorganic Chemistry, Faculty of Chemical Engineering and Technology, University of Zagreb, Marulićev trg 19, 10000 Zagreb, Croatia; pkassal@fkit.hr
[4] NMR Centre, Ruđer Bošković Institute, Bijenička cesta 54, 10000 Zagreb, Croatia; ana.cikos@irb.hr
[5] Laboratory for the Computational Design and Synthesis of Functional Materials, Division of Organic Chemistry and Biochemistry, Ruđer Bošković Institute, Bijenička cesta 54, 10000 Zagreb, Croatia
* Correspondence: mhranjec@fkit.hr (M.H.); robert.vianello@irb.hr (R.V.)

Abstract: We present the synthesis and analytical, spectroscopic and computational characterization of three amino-substituted benzo[*b*]thieno[2,3-*b*]pyrido[1,2-*a*]benzimidazoles as novel pH probes with a potential application in pH-sensing materials. The designed systems differ in the number and position of the introduced isobutylamine groups on the pentacyclic aromatic core, which affects their photophysical and acid-base properties. The latter were investigated by UV-Vis absorption and fluorescence spectroscopies and interpreted by DFT calculations. An excellent agreement in experimentally measured and computationally determined pK_a values and electronic excitations suggests that all systems are unionized at neutral pH, while their transition to monocationic forms occurs at pH values between 3 and 5, accompanied by substantial changes in spectroscopic responses that make them suitable for detecting acidic conditions in solutions. Computations identified imidazole imino nitrogen as the most favorable protonation site, further confirmed by analysis of perturbations in the chemical shifts of ^{1}H and ^{13}C NMR, and showed that the resulting basicity emerges as a compromise between the basicity-reducing effect of a nearby nitrile and a favorable contribution from the attached secondary amines. With this in mind, we designed a system with three amino substituents for which calculations predict pK_a = 7.0 that we suggest as an excellent starting point for a potential pH sensor able to capture solution changes during the transition from neutral towards acidic media.

Keywords: benzo[*b*]thieno[2,3-*b*]pyrido[1,2-*a*]benzimidazoles; DFT calculations; TD-DFT calculations; pH sensitivity; acid-base chemistry; NMR chemical shifts

1. Introduction

Nitrogen-containing heterocycles are, besides their well-known biological features, recognized as an interesting class of organic fluorescent sensors present in a wide range of biological, environmental, and chemical processes [1–4]. Owing to their excellent spectroscopic properties, as well as pronounced and diverse spectral responses, such derivatives offer promising applications in optoelectronics as optical lasers, fluorescence probes, organic luminophores or fluorescent dyes [5–8]. Among many heterocyclic derivatives developed as fluorescent organic sensors, benzimidazole derivatives play an important role and represent a special interest for organic chemists because of their eminent physico-chemical and spectroscopic characteristics [9,10]. Additionally, the benzimidazole framework, due to its

structural similarity to naturally occurring purines, is widely incorporated in the structure of numerous biologically important natural and synthetic molecules and could interact with important biomacromolecules within living organisms [11–13].

Furthermore, benzannulated benzimidazoles, due to condensation with other heteroaromatics, have a highly conjugated aromatic planar chromophore and thus exhibit bright fluorescence, which opens the possibility for their application as fluorescent chemosensing molecules, luminophores or dyes [14,15]. More importantly, the fluorescence intensity can be easily tuned by different substituents placed around the heteroaromatic skeleton, allowing for their application as fluorescent pH sensors. In recent years, fluorescent sensors have been actively investigated because of their high sensitivity and rapid responses to various analytes, among which pH probes could be used for a wide range of conditions, including extremely acidic and basic environments [16–19]. Recently, we studied spectroscopic characteristics of tetracyclic benzimidazole derivatives, among which 2-amino-5-phenylbenzimidazo[1,2-*a*]quinoline-6-carbonitrile has proven to be selective towards Zn^{2+} concomitant, with a significant increase in fluorescence intensity [20]. Encouraged by these findings, we have chosen several biologically active benzimidazo[1,2-*a*]quinolines bearing amino substituents on different positions (Figure 1) to study their optical properties and possible application as pH sensors through UV-Vis and fluorescence spectroscopies and computations. The study of their acid-base properties underlined that all examined compounds showed spectral changes in the pH range of 1–12, with very strong sensitivity of fluorescence towards pH, thus confirming the requirements for efficient pH sensors [21,22].
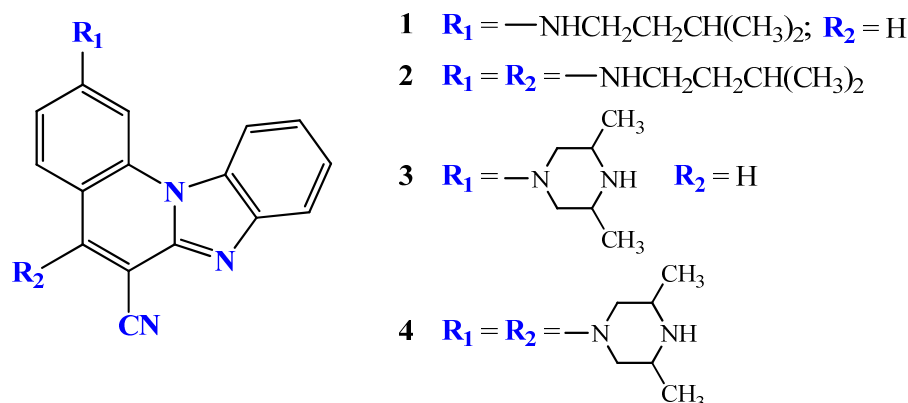

1 $R_1 = $ —NHCH$_2$CH$_2$CH(CH$_3$)$_2$; $R_2 = $ H

2 $R_1 = R_2 = $ —NHCH$_2$CH$_2$CH(CH$_3$)$_2$

3 $R_1 = $ $R_2 = $ H

4 $R_1 = R_2 = $

Figure 1. Recently studied benzimidazo[1,2-*a*]quinolones.

Pentacyclic benzo[*b*]thieno[2,3-*b*]pyrido[1,2-*a*]benzimidazoles with amino chains at different positions, recently synthesized in our research group, have been evaluated by 2D and 3D assays on human breast cancer cells, showing very promising biological potential [23]. The general structure of these dye molecules is based on a fused and highly conjugated planar chromophore system containing five fused heteroaromatic cores, showing excellent optical properties, including strong fluorescence in the visible spectrum (around 500 nm), as well as good photostability. In this work, the pH sensitivity of their spectroscopic properties was studied by UV-Vis and fluorescence spectroscopy, showing that the protonation-deprotonation equilibrium of the dyes is associated with drastic changes in photophysical properties that could be harnessed for practical applications. Computational analysis revealed that all system exchange between neutral and monoprotonated forms in the range of 3 < pH < 5, while excited-state calculations reproduced experimental spectra and further confirmed that the observed spectral alterations are brought about by this process. Analysis of perturbations in the chemical shifts of ^{1}H and ^{13}C NMR was used to additionally support the protonation state change with varying pH but also to identify the exact protonation site within the molecule.

2. Materials and Methods

2.1. General Methods for Synthesis

All chemicals p.a. purity and reagent-grade solvents were purchased from commercial suppliers Aldrich and Acros. Melting points were recorded on SMP11 Bibby and Büchi 535 apparatus and are uncorrected. Deuterated solvents for NMR analysis were purchased from EuroIsotop. 1D and 2D NMR spectra were recorded on Bruker Avance AV300 and AV600 spectrometers equipped with a 5 mm diameter BBO probe with z-gradient accessory. All spectra were acquired with standard Bruker pulse sequences on samples in DMSO-d_6 and 90% DMSO-d_6/10% D_2O at 25 °C, using TMS as internal standard. Chemical shifts are reported in ppm (δ) relative to TMS or to a deuterated solvent when TMS was not visible. Analytical thin-layer chromatography was performed with commercial Merck silica gel 60F-254 glass plates. By using multifunctional MW reactor Milestone start S and quartz cuvettes, the uncatalyzed microwave-assisted amination was conducted under the pressure of 40 bar and 180 °C. Agilent 1200 series LC/6410 QQQ instrument was used to record mass spectra at room temperature.

2.2. General Method for Preparation of Compounds 4–6

Amino-substituted targeted pentacyclic derivatives 4–6 were prepared according to the previously published experimental procedures from corresponding halogeno- and dihalogeno-substituted precursors within the microwave-assisted uncatalyzed amination by using an excess of isobutylamine in acetonitrile [23].

2.2.1. 3-*N*-*i*-butylaminobenzo[*b*]thieno[2,3-*b*]pyrido[1,2-*a*]benzimidazole-7-carbonitrile **4**

Compound 4 was prepared using the method described above from 1 (100 mg, 0.32 mmol) and *i*-butylamine (1.20 mL, 24.44 mmol) after 13 h of irradiation to yield 632 mg (27%) of orange powder; m.p. 247–252 °C. ^{1}H NMR (DMSO-d_6, 300 MHz): δ/ppm = 8.76 (s, 1H, H$_{arom.}$), 8.58 (d, 1H, *J* = 5.76 Hz, H$_{arom.}$), 8.55 (d, 1H, *J* = 6.81 Hz, H$_{arom.}$), 7.98 (d, 1H, *J* = 8.04 Hz, H$_{arom.}$), 7.62 (t, 1H, *J* = 7.62 Hz, H$_{arom.}$), 7.47 (t, 1H, *J* = 7.80 Hz, H$_{arom.}$), 7.23 (d, 1H, *J* = 2.01 Hz, H$_{arom.}$), 7.04 (dd, 1H, J_1 = 2.16 Hz, J_2 = 9.29 Hz, H$_{arom.}$), 6.97 (t, 1H, *J* = 5.67 Hz, NH), 3.02 (t, 2H, *J* = 6.23 Hz, CH$_2$), 1.95 (m, 1H, CH), 0.99 (d, 6H, *J* = 6.60 Hz, CH$_3$); ^{13}C NMR (DMSO-d_6, 150 MHz): δ/ppm = 150.1, 146.9, 145.2, 144.2, 135.9, 133.1, 129.5, 125.7, 124.9, 120.8, 119.6, 118.1, 117.2, 116.5, 114.9, 113.7, 101.7, 93.5, 50.2, 27.2, 20.3 (2C); Found: C, 71.34; H, 4,89; N, 15.11. Calc. for $C_{22}H_{18}N_4S$: C, 71.32; H, 4.90; N, 15.12%.

2.2.2. 6-*N*-*i*-butylaminobenzo[*b*]thieno[2,3-*b*]pyrido[1,2-*a*]benzimidazole-7-carbonitrile **5**

Compound 5 was prepared using the method described method from 2 (100 mg, 0.30 mmol) and *i*-butylamine (0.35 mL, 3.50 mmol) after 3 h of irradiation to yield 74 mg (67%) of yellow powder; m.p. 198–1202 °C. ^{1}H NMR (DMSO-d_6, 300 MHz): δ/ppm = 8.75 (d, 1H, *J* = 9.03 Hz, H$_{arom.}$), 8.30 (dd, 2H, J_1 = 2.01 Hz, J_2 = 8.67 Hz, H$_{arom.}$), 7.91 (t, 1H, *J* = 6.18 Hz, NH), 7.78 (d, 1H, *J* = 7.74 Hz, H$_{arom.}$), 7.74–7.67 (m, 2H, H$_{arom.}$), 7.45 (t, 1H, *J* = 7.35 Hz, H$_{arom.}$), 7.31 (t, 1H, *J* = 7.26 Hz, H$_{arom.}$), 3.64 (t, 2H, *J* = 6.72 Hz, CH$_2$), 2.23–2.09 (m, 1H, CH), 1.00 (d, 6H, *J* = 6.60 Hz, CH$_3$); ^{13}C NMR (DMSO-d_6, 75 MHz): δ/ppm = 151.1, 148.2, 144.7, 138.5, 133.0, 130.0, 128.8, 128.0, 125.1, 124.3, 124.1, 124.1, 119.5, 118.4, 117.5, 117.2, 114.0, 71.6, 50.7, 28.3, 19.4 (2C); Found: C, 71.30; H, 4,91; N, 15.15. Calc. for $C_{22}H_{18}N_4S$: C, 71.32; H, 4.90; N, 15.12%.

2.2.3. 3,6-di-(*N*-*i*-butylamino)benzo[*b*]thieno[2,3-*b*]pyrido[1,2-*a*]benzimidazole-7-carbonitrile **6**

Compound 6 was prepared using the method described above from 3 (100 mg, 0.28 mmol) and *i*-butylamine (1.25 mL, 12.37 mmol) after 27 h of irradiation to yield 24 mg (19%) of yellow powder; m.p. 144–148 °C. ^{1}H NMR (DMSO-d_6, 300 MHz): δ/ppm = 8.42 (d, 1H, *J* = 9.15 Hz, H$_{arom.}$), 8.26 (d, 1H, *J* = 8.22 Hz, H$_{arom.}$), 7.73 (d, 1H, *J* = 7.86 Hz, H$_{arom.}$), 7.58 (t, 1H, *J* = 6.26 Hz, NH), 7.42 (t, 1H, *J* = 7.61 Hz, H$_{arom.}$), 7.27 (t, 1H, *J* = 7.76 Hz, H$_{arom.}$), 7.20 (d, 1H, *J* = 1.92 Hz, H$_{arom.}$), 7.01 (dd, 1H, J_1 = 1.97 Hz, J_2 = 9.20 Hz, H$_{arom.}$), 6.76 (t, 1H,

J = 5.30 Hz, NH), 3.60 (t, 2H, J = 6.63 Hz, CH$_2$), 3.00 (t, 2H, J = 6.14 Hz, CH$_2$), 2.19–2.06 (m, 1H, CH), 2.00–1.86 (m, 1H, CH), 0.99 (d, J = 4.68 Hz, 6H, CH$_3$), 0.97 (d, J = 4.62 Hz, 6H, CH$_3$); ^{13}C NMR (DMSO-d_6, 75 MHz): δ/ppm = 151.0, 150.2, 149.0, 145.3, 142.8, 134.8, 130.4, 125.3, 124.6, 119.6, 118.6, 118.4, 118.2, 114.3, 113.9, 111.7, 102.1, 70.3, 51.2, 50.6, 28.9, 27.8, 20.7 (2C), 19.9 (2C); Found: C, 70.74; H, 6.17; N, 15.85. Calc. for C$_{26}$H$_{27}$N$_5$S: C, 70.72; H, 6.16; N, 15.86%.

2.3. Spectroscopic Characterization

A Varian Cary 50 spectrophotometer in double-beam mode was used to record the UV-Vis absorption spectra in methanol of reagent grade in the wavelength range of 200–650 nm at room temperature. The absorbance values were recorded with a 0.1 nm resolution using transparent quartz cuvettes of 1 cm path length. Emission spectra were taken on a Varian Cary Eclipse spectrophotometer, also at room temperature, with quartz cells of 1 cm path length. Excitation spectra in the range of 200–500 nm revealed the excitation maxima necessary to record the emission spectra between 400 and 600 nm. Fluorescence spectra were corrected for the effects of time- and wavelength-dependent light-source fluctuations. For the correction, standard of rhodamine 101, a diffuser provided with the instrument, as well as the instrument software, was used.

2.4. pH Titrations

In order to study the changes in the spectroscopic characteristics of 4–6 obtained within the usage of reagent-grade universal buffers with different pH values within pH = 1–13, room-temperature UV-Vis and fluorescence emission spectra were recorded. Amounts of 0.1 M pH buffer solutions were prepared using boric acid, citric acid, phosphoric acid and sodium hydroxide, and pH was adjusted with hydrochloric acid. As terminal acidic and basic points in the titration experiments, solutions of 0.1 mol dm^{-3} hydrochloric acid (for pH = 1) and 0.1 mol dm^{-3} sodium hydroxide (for pH = 13) were used. The employed concentrations of systems 4–6 were 1×10^{-5} mol dm^{-3} for the UV-Vis and 5×10^{-8} mol dm^{-3} (4), 5×10^{-7} mol dm^{-3} (5), 1×10^{-7} mol dm^{-3} (6) for the fluorescence measurements. The excitation wavelengths were determined from the absorption spectra. pK_a values for 4 and 6 were determined from ratiometric fluorescence titrations by calculating the ratio of fluorescence intensities at the wavelengths of acidic and basic emission maxima. Due to the relatively lower fluorescence intensities, the pK_a value for **5** was determined from UV-Vis absorption spectra, using the absorbance maximum in acidic conditions [24].

2.5. Analysis of Perturbations in NMR Chemical Shifts

A total of 5.8 mg of 5 was added to the solution mixture of 540 μL reagent-grade DMSO-d_6 and 60 μL reagent-grade D$_2$O. The final pD of the sample was measured to be 7.1. Considering the correction of 0.4 units for the change in the glass-electrode potential because of D$_2$O, the actual pH was estimated to be 7.5. A total of 6.0 mg of 5 was added to the solution mixture of 540 μL DMSO-d_6 and 60 μL of 1 mol dm^{-3} DCl in D$_2$O. The final pD of the sample was measured to be 2.0. Employing the same 0.4-unit correction, the actual pH was estimated to be 2.4. The complete ^{1}H and ^{13}C assignments were made on the basis of one- and two-dimensional NMR spectra (^{1}H, ^{13}C, COSY, HSQCe and HMBC). All spectra and their acquisition parameters can be seen in Supplementary Information.

2.6. Computational Details

For ground-state calculations, all molecular geometries were optimized using a very efficient B3LYP/6–31+G(d) model, which was designed to provide highly accurate thermodynamic and kinetic parameters for various organic systems, in line with our earlier work [9,21]. To account for the solvent effects, during geometry optimization, we included the implicit SMD solvation model corresponding to pure solvents [25]. Thermal corrections were extracted from the corresponding frequency calculations so that all value pertain to
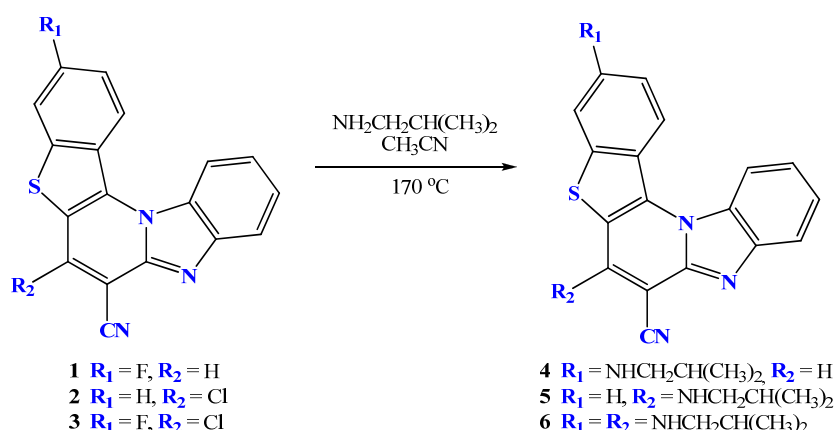
Gibbs free-energy differences at room temperature and normal pressure. The selection of such a computational approach was motivated by its accuracy in evaluating the reaction parameters and pK_a values for a variety of analogous organic systems [26,27]. In this work, pK_a parameters were obtained in an absolute way using the proton's gas phase free energy of G$^\circ$(H$^+$) = 6.28 kcal mol^{-1} and its experimental aqueous-solution solvation free energy of ΔG_{SOLV}(H$^+$) = -265.9 kcal mol^{-1} [28], also employed by Truhlar and colleagues [25] in parameterizing the utilized SMD model. The latter value incorporates a constant term of -1.89 kcal mol^{-1} associated with the change in the free energy on moving from a gas-phase pressure of 1 atm to a liquid-phase concentration of 1 M.

For excited-state calculations, geometries of the ground and lowest excited states were optimized with DFT and time-dependent DFT approaches, respectively, with the B3LYP functional and 6–31+G(d,p) basis set. Dispersion interactions were accounted for by the empirical method D3 [29], while solvation effects were implicitly introduced through the SMD model [25]. The emission energies of the excited-state optimized geometries were calculated with solvent equilibration through external iterations. For the final excited-state energies, a larger basis set, 6–311++G(2d,2p), was used. The calculated geometries and UV-Vis spectra were visualized with the GaussView program [30]. All calculations were performed with the Gaussian 16 package [31].

3. Results and Discussion

3.1. Chemistry

All studied pentacyclic benzo[*b*]thieno[2,3-*b*]pyrido[1,2-*a*]benzimidazoles were prepared by the uncatalyzed microwave-assisted amination from the corresponding halogeno/dihalogeno-substituted precursors (Scheme 1) according to previously published synthetic procedures [23]. The obtained compounds were purified using silica-gel column chromatography, while their structures were determined through inspection of H–H coupling constants and chemical shifts derived from NMR spectra, as well as identification of the molecular ions with mass spectrometry. A downfield shift of the aromatic protons could be observed in ^{1}H NMR spectra when compared to the spectra of halogeno-substituted precursors. Additionally, the signals related to the amino substituents are visible in the aliphatic region of both ^{1}H and ^{13}C spectra.

1 R$_1$ = F, R$_2$ = H
2 R$_1$ = H, R$_2$ = Cl
3 R$_1$ = F, R$_2$ = Cl

4 R$_1$ = NHCH$_2$CH(CH$_3$)$_2$, R$_2$ = H
5 R$_1$ = H, R$_2$ = NHCH$_2$CH(CH$_3$)$_2$
6 R$_1$ = R$_2$ = NHCH$_2$CH(CH$_3$)$_2$

Scheme 1. Synthesis of amino-substituted pentacyclic benzimidazole derivatives.

3.2. Spectroscopic Characterization

To investigate photophysical features of prepared systems, UV-Vis and fluorescence emission spectra were recorded in methanol. The main focus was to study the influence of amino substituent position at the pentacyclic skeleton on spectroscopic characteristics.

3.2.1. UV-Vis Absorption Spectra

UV-Vis spectra were recorded at room temperature in methanol in the range of 200–600 nm at the same concentration of 2×10^{-5} mol dm^{-3} for all derivatives (Figure 2).
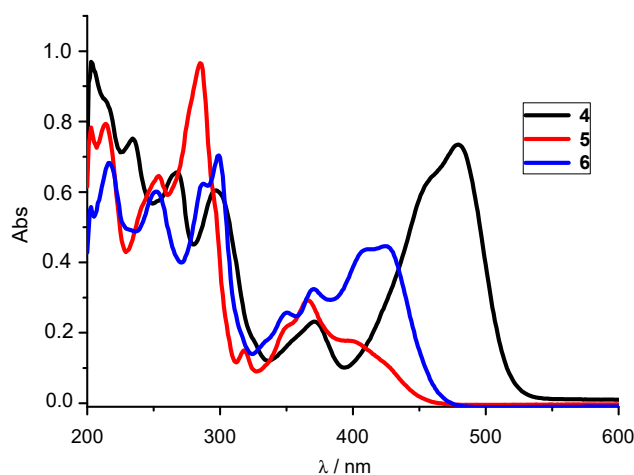
Figure 2. UV-Vis spectra of systems 4–6 recorded in methanol at concentration of 2×10^{-5} mol dm^{-3}.

The UV-Vis spectra of 4–6 show one main absorption band, which, for 5 and 6, is centered at 330–470 nm and at 400–520 nm for 4. Based on computational results, these bands were assigned to π–π* transitions (Figures S16, S18 and S20). On the same grounds, the absorption bands in the region from 250 to 330 nm were assigned to the transitions within the pentacyclic conjugated aromatic π-system. The most intensive absorbance with a strong hyperchromic effect and a strong bathochromic shift was observed for 4, relative to 5 and 6, while system 5 showed a hypsochromic shift of the absorption maxima, as well as a hypochromic effect.

3.2.2. Fluorescence Emission Spectra

Emission spectra were measured between 400 and 700 nm at the concentrations of 5×10^{-8} mol dm^{-3} (4), 5×10^{-7} mol dm^{-3} (5) and 1×10^{-7} mol dm^{-3} (6) at room temperature (Figure 3).

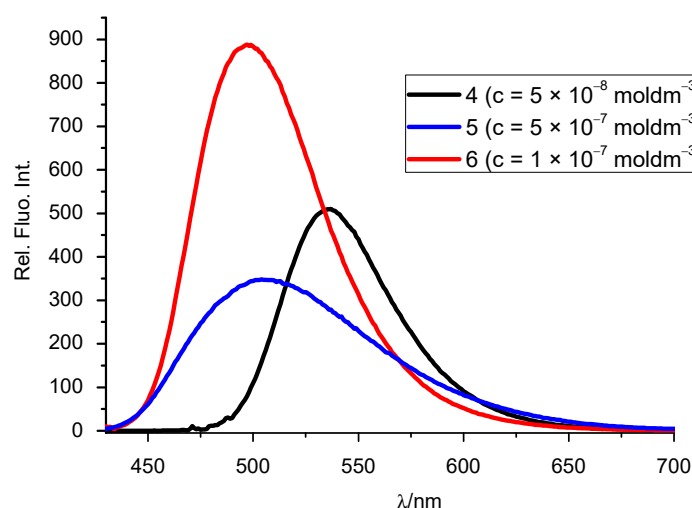**Figure 3.** Emission spectra of 4–6 in methanol ($\lambda_{exc.}(4) = 479$ nm; $\lambda_{exc.}(5) = 319$ nm; $\lambda_{exc.}(6) = 425$ nm).

Emission spectra of all systems reveal one main emission band. Diamino-substituted 6 showed a slight hypsochromic shift relative to monosubstituted 5, while system 4, bearing isobutylamine substituent at position 3, exhibited significant bathochromic shift relative to 5 and 6. System 4 showed the greatest fluorescence intensity (note the lower concentration), followed by 6, while 5 showed the lowest fluorescence intensity when compared to other derivatives. Electronic absorption and fluorescence data for 4–6 are summarized in Table 1.

Table 1. Electronic absorption and fluorescence emission data for systems 4–6.

System	λ_{max} (nm)	$\varepsilon \times 10^3$ (dm^3 mol^{-1} cm^{-1})	λ_{emis} (nm)	Rel. Fluorescence Int.
4	479	36.6	536	512
	459	32.3		
	371	11.45		
	297	30.05		
	267	32.7		
	234	37.4		
5	401	8.8	505	347
	367	14.5		
	319	7.2		
	285	48.1		
	253	32.1		
6	425	22.2	498	885
	412	21.9		
	370	16.35		
	350	12.85		
	230	35.2		
	287	31.15		
	252	30.0		

3.3. Effects of pH on Spectral Properties

Aqueous-solution pK_a values are useful parameters to determine precise protonation states of a molecule and are typically used to characterize potential optical pH sensors. Optical evaluation of the concentrations of the acidic (HA) and basic forms (A$^-$) is based on the Henderson—Hasselbach equation [32]:

$$pH = pK_a + \log \frac{[A^-]}{[HA]} \tag{1}$$

pH dependence of spectral properties was inspected by spectroscopic pH titrations. Through the protonation of the basic nitrogen within the pentacyclic skeleton, pronounced spectral changes were observed, thereby confirming the potential of the studied systems as pH-sensing optical probes (Figure 4 for 4, Figure S1 for 5–6). When compared, the effect of pH is more evident in the fluorescence spectra than in the absorption. The binding of a proton alters π-conjugation and electronic features of the aromatic moieties, which results in changed both emission intensity and color. In addition, protonation causes a hypsochromic shift (blue shift) of absorption bands for all systems (Table 2).

Table 2. pH dependence of absorption and fluorescence emission for 4–6 in buffered solutions [1].

	λ_{max} (nm)			$\varepsilon \times 10^3$ (dm^3 mol^{-1} cm^{-1})			λ_{emis} (nm)			Stokes Shift (nm)			pK_a
	Acidic	Neutral	Basic	Acidic	Neutral	Basic	Acidic	Neutral	Basic	Acidic	Neutral	Basic	
4	491	499	494	14.40	8.30	7.40	571	548	551	80	49	57	3.01
	378	469	466	4.60	9.05	8.55							
		377			4.45	4.05							
5	356	447	443	16.05	11.30	12.05	511	524	517	155	77	74	3.18
		385	380		12.05	13.55							
		313	311		15.35	18.80							
6	416	444	446	5.90	10.70	12.25	527	513	512	111	69	66	4.73
	361	415	416	10.75	9.85	11.15							
		377	378		8.95	10.15							

[1] Acidic, neutral and basic conditions are 0.1 M HCl, MQ water and buffer at pH = 13, respectively.

Representative spectral responses to varied pH for 4 are shown in Figure 4. As seen, a significant increase in the absorbance and fluorescence intensity occurs on moving from neutral to acidic conditions, while in alkaline media, the changes are practically negligible. Additionally, only one absorption band with a maximum at 491 nm is visible in the acidic environment, where the emission spectra maxima showed a bathochromic shift of around 23 nm. System 6 exhibited similar behavior: a bathochromic shift and increased fluorescence

in acidic media. Interestingly, only 5 showed a hypochromic shift of emission intensity in acidic conditions relative to neutral and basic media, as well as a hypsochromic shift of emission maxima around 13 nm (Figure S1). Stokes shifts (Table 2) are moderate in neutral and basic media for all systems (49–77 nm) but are exceptionally high in acidic media, reaching a maximum of 155 nm for 5. This is significant for a potential application of these systems as fluorescent pH sensors in acidic aqueous solutions.
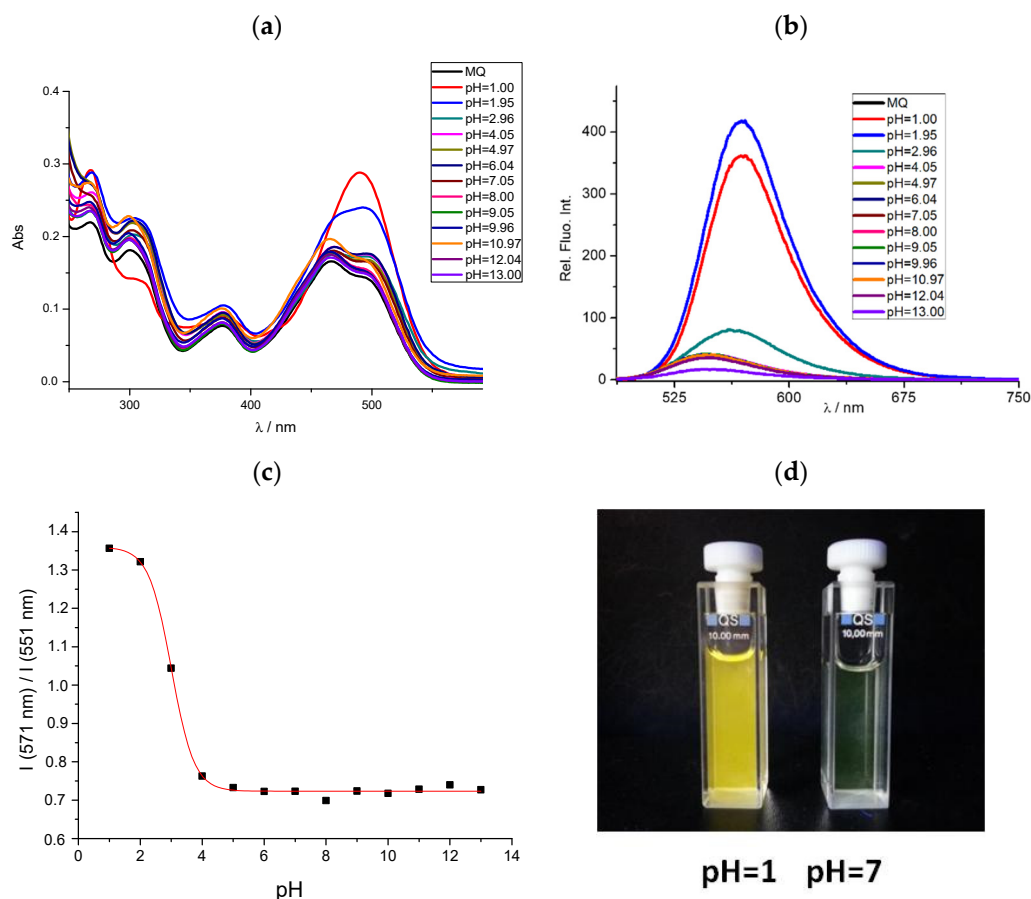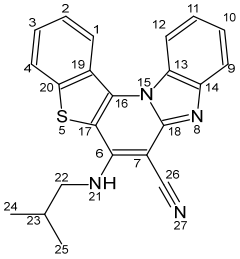
Figure 4. Absorption (**a**) and emission (**b**) spectra for 4 at different pH values in buffer (λ_{exc} = 467 nm). (**c**) Ratiometric fluorescence pH titration curve from which the pK_a value was obtained and (**d**) its photos at pH = 1 and pH = 7 under UV lamp (365 nm).

The acid-base features are best described by an 'apparent' pK_a value, as opposed to a real thermodynamic pK_a, since pH titrations were not performed under strictly controlled temperature and ionic strength. The pK_a values were determined as the inflection point of a sigmoid Boltzmann curve fitted to the experimental pH titration data. As seen in Table 2, the obtained apparent pK_a values are 3.01, 3.18 and 4.73 for 4–6, respectively. A single pK_a was obtained for each system, indicating that they all exist in two different states in the tested pH range (2–13), which is confirmed by the computational analysis (see later).

3.4. Effects of pH on NMR Spectra

Since spectroscopic pH titrations showed that 5 changes the protonation state at pH around 3, our idea was to record and analyze NMR spectra in neutral and acidic media, aiming to identify which nitrogen atom becomes protonated under acidic conditions. Initially, we were thinking of comparing ^{15}N chemical shifts at pH = 2 and pH = 7, but the solubility of 5 in water proved to be insufficient. Instead, we performed the analysis in solvent mixture of 90% DMSO-d_6/10% D_2O and monitored the effect of protonation on ^{1}H and ^{13}C chemical shifts (Table 3). Therefore, two samples of 5 were prepared, one at pH = 7.5 and the other at pH = 2.4. All recorded NMR spectra are shown in Figures S2–S11.

Table 3. Proton and carbon NMR chemical-shift comparison for 5 under neutral and acidic conditions, all in 90% DMSO-d_6/10% D_2O at 25 °C. The largest differences in chemical shifts are marked as bold. Indicated positions correspond to the presented atom numbering.

Position	Proton Chemical Shifts (ppm)			Carbon Chemical Shifts (ppm)		
	pH = 7.5	pH = 2.4	Δ	pH = 7.5	pH = 2.4	Δ
1	8.76	8.62	0.13	124.63	125.10	0.47
2	7.70	7.72	0.02	125.72	126.27	0.55
3	7.20	7.79	0.07	128.75	129.95	1.20
4	8.26	8.33	0.07	124.47	124.68	0.21
6				148.67	150.71	2.05
7				71.75	68.55	−3.20
9	7.77	7.82	0.05	**118.80**	**113.90**	−4.90
10	**7.46**	**7.68**	**0.22**	124.95	127.78	2.82
11	**7.32**	**7.57**	**0.25**	120.22	123.80	3.58
12	8.30	8.37	0.06	114.51	115.97	1.46
13				130.41	128.47	−1.94
14				**144.86**	**132.40**	−12.46
16				133.50	133.23	−0.27
17				117.65	115.09	−2.55
18				151.53	148.53	−3.01
19				129.23	128.45	−0.78
20				138.87	139.70	0.83
22	3.62	3.66	0.05	50.94	51.17	0.23
23	2.12	2.13	0.01	28.73	28.99	0.26
24,25	0.97	0.98	0.02	19.71	19.67	−0.04
26				117.89	120.70	2.80

Data in Table 3 and Figure 5a clearly indicate that the biggest difference between the spectra recorded in neutral and acidic conditions is observed for proton chemical shifts H-10 and H-11. Both protons show a significant downfield shift in the protonated form, which agrees with previously published work in similar systems [33]. This narrows down the possible protonation site to the benzimidazole unit, the final choice being either N-8 or N-15. Further analysis of carbon chemical shifts at different pH values (Table 3 and Figure 5b) revealed the biggest difference for C-9 and C-14 resonance lines. As previously shown for several benzimidazoles [33], the largest upfield shift for carbon signals is expected for the resonance line of the carbon adjacent to the protonation site. In our case, the 12.46 ppm upfield shift was found for C-14, which identifies imidazole N-8 as the most probable protonation site, in line with computations presented later.

3.5. Computational Analysis

3.5.1. Acid-Base Properties

Computational analysis was performed to offer an insight into the acid-base features of studied systems and to provide interpretation of the observed spectroscopic properties in solution. Initially, we focused on calculating the matching pK_a values (Table 4), which reveal an excellent agreement with experiments. Specifically, for 4–6, relative differences between computed and measured data are only 0.2, 0.3 and 0.7 pK_a units, respectively, which strongly confirms the validity of the employed computational approach.
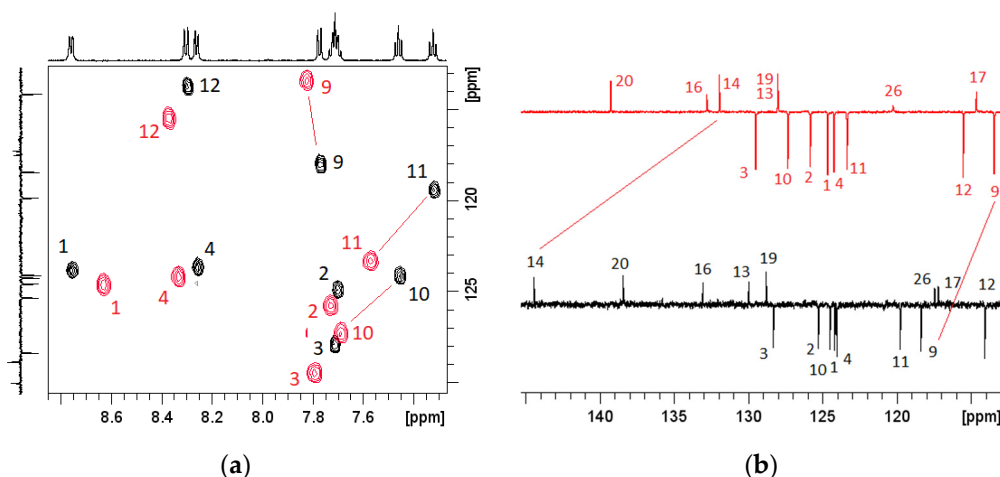
Figure 5. Comparison of ^{1}H-^{13}C HSQC (**a**) and ^{13}C NMR spectra (**b**) for 5 showing the biggest differences in chemical shifts between the neutral (pH = 7.5, black) and acidic (pH = 2.4, red), all in 90% DMSO-d_6/10% D$_2$O at 25 °C. Atom numbering is used in accordance with Table 3.

Table 4. Calculated aqueous-phase pK_a values at the (SMD)/B3LYP/6–31+G(d) level of theory. Experimental values determined in this work are given in square brackets for comparison.

System	Protonation State	pK_a(calc)	Protonation Reaction
	4^-	24.2	N2$^-$ → N2–H
	4	3.2 [3.01]	N1 → N1–H$^+$
	4^+	−1.3	N2 → N2–H$^+$
	5^-	17.0	N2$^-$ → N2–H
	5	3.9 [3.18]	N1 → N1–H$^+$
	5^+	−14.1	N2 → N2–H$^+$
	6^{2-}	28.5	N3$^-$ → N3–H
	6^-	18.4	N2$^-$ → N2–H
	6	5.0 [4.73]	N1 → N1–H$^+$
	6^+	−1.0	N3 → N3–H$^+$
	6^{2+}	−13.9	N2 → N2–H$^+$

Considered systems are composed of five cyclic units, encompassing the imidazole and thiophene rings as likely sites for protonation. Still, it turns out that the most basic position in 4–6 is imidazole imino nitrogen, which is, not surprisingly, given a typically higher basicity of nitrogen heterocycles than their sulfur analogues in the aqueous solution [34]. In addition, imidazole (pK_a = 6.95) and benzimidazole (pK_a = 5.56) are more basic than aniline (pK_a = 4.62) and *N*-methylaniline (pK_a = 4.85) [34], which further confirms imidazole N-atom as the most susceptible towards protons.

Our analysis identifies that systems 4–6 are unionized under neutral conditions since imidazole protonation occurs under acidic conditions with pH values equal to or lower than 5. Comparing the systems with a single amino substituent, the basicity of 5 surpasses that of 4, in agreement with experiments, because of a higher positive electron-donating influence of the N-alkyl unit in the former and due to the closer proximity to the protonation

site in 5 relative to 4. Disubstituted 6 combines the favorable effect of both N-alkyl groups, and the resulting basicity is higher, at $pK_a = 5.0$, in line with experiments.

The second protonation in all systems occurs at pH values below zero, which would require extremely acidic conditions for it to be allowed. This suggests that dicationic systems are not predominant protonation forms under conditions employed in this work, although a notable portion of diprotonated 4-H^{++} and 6-H^{++} is possible at the lowest pH values. Specifically, considering $pK_a = -1.0$ for the second protonation of 6 indicates that at pH = 1, there is around 4% of 6-H^{++} in solution, which becomes important for rationalization of its excitation spectra (see latter). In addition, one observes a very low amine basicity in 5 of around 13 pK_a units lower than in 4 and 6 because of the presence of a vicinal –CN group, which is known to be among the most efficient acidifiers and basicity-reducing groups [35,36]. This is also the reason why a more distant amine substituent in 6 is more basic than that of its analogue placed closer to the nitrile.

Where potential deprotonation reactions are concerned, the highest acidities reside on the secondary N–H amino groups, yet the calculated pK_a values are located beyond employed experimental conditions, thereby disallowing the existence of monoanionic species in our case. In terms of basicities, 5 is more acidic than 4 since its deprotonating amine is positioned closer to the favorable effect of the electron-withdrawing –CN group, while the same argument can be used to interpret the acidity trend among amines in disubstituted 6.

In concluding this section, we can emphasize that at neutral pH, 4–6 are all present as unionized systems, while under employed experimental conditions (pH = 1–13) they interchange with monocationic derivatives protonated at the imidazole N-atom at pH values between 3 and 5. Our analysis also reveals that investigated systems are less basic than both imidazole and benzimidazole. Considering the relative difference between the latter two reference systems, a reduction in the basicity of 4–6 comes as a result of a further annulation that depletes the electron density from N-atoms but also because of the nearby presence of an efficient basicity-reducing, electron-withdrawing –CN group. The latter overcomes a favorable influence of the attached secondary amines, even when two such moieties are introduced in 6. To test these hypotheses, we repeated the analysis on three systems 7–9 (Figure 6), with the additional idea to bring the corresponding pK_a values closer to 7, which would be beneficial for their practical application. When the most basic 6 is depleted from the –CN group, as in 7, the basicity of the system, expectedly, increases to $pK_a = 9.2$, thus confirming the unfavorable effect of the latter moiety. Along these lines, if 7 is enriched with another amine moiety, this time placed on the benzimidazole part of the system, as in 8, the resulting basicity is additionally increased to $pK_a = 11.5$, which would promote both 7 and 8 as efficient pH sensors for alkaline media. Lastly, if this strategy is combined, as in 9, which maintains the nitrile group as an important building requirement during the employed synthetic approach, while having additional amine relative to 6, the resulting pK_a value assumes precisely $pK_a = 7.0$. This suggests that system 9 bears acid/base features with significant practical usefulness, which, provided it shows appropriate analytic responses, would make it an applicable pH sensor for acidic media below neutrality. Because of that, its synthesis and characterization remain challenges for future studies.
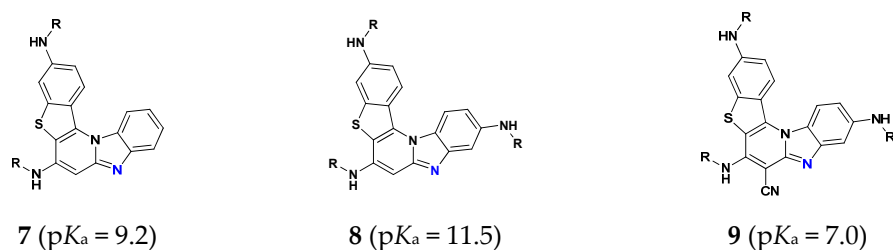

7 ($pK_a = 9.2$)   **8** ($pK_a = 11.5$)   **9** ($pK_a = 7.0$)

Figure 6. Systems investigated computationally (R = isobutyl) and the calculated pK_a values in water corresponding to the protonation of the imidazole imino nitrogen, indicated in blue.

3.5.2. Absorption and Emission Spectra

Variations in pH conditions are remarkably reflected in the UV-Vis absorption and emission spectra of 4–6. By comparing the calculated spectra of the chemical species potentially present at different pH values with experiments, it is possible to recognize the protonation forms responsible for the detected spectral changes (Figures S12–S15).

The absorption spectra generated from the calculated vertical excitation states of neutral 4–6 (Figure 7) are in very good agreement with experimental measurements (Figure 2). This confirmed the basic reliability of the calculation methods and the theoretical characterization of the spectra. Representation of the lowest excited states for all the involved chemical species (neutral and protonated) in terms of the natural transition orbitals (NTO) [37] shows that these excitations can be clearly classified as the π–π* transitions (Figures S16–S22). Mostly, they are well described by only one pair of NTOs, with the unoccupied one being very similar to the canonical LUMO orbital.
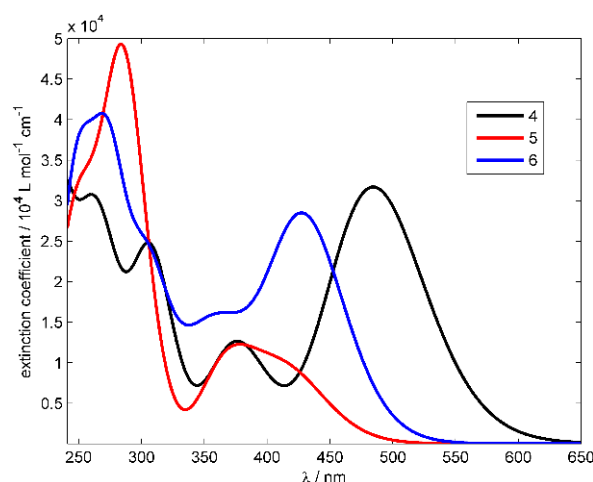
Figure 7. Calculated UV-Vis absorption spectra for systems 4–6 obtained through (SMD)/B3LYP/6–311++G(2d,2p)//(SMD)/B3LYP/6–31+G(d,p) calculations.

The changes in the absorption spectra due to pH variation are explained by the equilibrium dynamics between neutral 4–6 and their protonated derivatives. On the other hand, the calculations for deprotonated anionic species (at the amino N–H group) suggest that they do not exist at the experimental range of pH values, which is consistent with the calculated pK_a data (Table 4). Indeed, the spectral shapes of 4–6 within pH = 7–14 are rather conserved, showing only minor changes, which can be assigned to different compositions of the buffer solutions. Remarkable shifts in the absorption bands occur in the acidic region of pH = 1–7 that are explained by assuming protonation of one or more nitrogen atoms. Indeed, excited state calculations for all potential protonated species and their comparison with experimental spectra, confirm that in all three systems the imidazole imino nitrogen accepts the proton most easily. In 4 and 5, only this atom is substantially protonated at pH = 1–7, but in 6, the amino-nitrogen at position 6 also becomes protonated at very low pH values. Specifically, dicationic 6 is required to match experimental data at such acidic conditions (Figure S15), being in line with the calculated protonation constants, which confirms the fact that the protonation of the amino group in 6 is at least partially feasible under employed experimental conditions.

The fluorescence spectra are commonly explained by assuming that emission occurs from the lowest excited state after geometrical relaxation (Kasha's rule) [38]. The calculated emission wavelengths for 4 and 4-H$^+$ are almost the same (539 nm and 538 nm), which is in reasonable agreement with experimental values of 546 nm and 569 nm recorded in the neutral medium and at pH = 1, respectively. The calculated emission wavelengths for 6 and 6-H^{++} are 541 nm and 565 nm, which reproduce the experimental trend of 514 nm and 527 nm for the neutral medium and at pH = 1, respectively, and do not deviate too

much in absolute values. Only for **5** and **5-H**[+], the calculated emission wavelengths of 678 nm and 640 nm, respectively, correctly reproduce the trend in experimental values yet somewhat disagree in quantitative terms with the emissions recorded at 518 nm and 508 nm in the neutral medium and at pH = 1, respectively. As the excitation wavelength is relatively high (310 nm), the emission may, in principle, occur not from the lowest but from a higher excitation state, although this is considered to rarely happen.

Geometrical relaxation in the first excited state does not bring significant changes in the structural parameters, likely because the conjugated π-skeleton is remarkably rigid. Although protonation induces visible changes only with amino-nitrogens as proton acceptors, these are still restricted to their local environment (Figures S23–S25).

Overall, the calculated absorption and emission spectra fully support the pH-dependent chemical speciation established by the calculated thermodynamic acid-base constants and the presented NMR evidence.

4. Conclusions

This work employs UV-Vis and fluorescence spectroscopies to describe the optical properties and pH-sensing ability of the prepared pentacyclic amino-substituted benzo[*b*] thieno[2,3-*b*]pyrido[1,2-*a*]benzimidazoles and reports their aqueous pK_a values through pH titrations in buffered water solutions.

The UV-Vis absorption spectra reveal one absorption band at 330–470 nm for **5** and **6**, which is shifted to 400–520 nm for **4**, and one emission band for all systems. The most intensive absorbance with a strong hyperchromic effect and a strong bathochromic shift was seen for **4**. Aqueous pK_a values appear suitable for monitoring acidic pH in solution, as differences in the electronic transitions occur at pH values between 3 and 5, where all systems change from unionized to monoprotonated forms. This is supported by DFT calculations, which achieved excellent agreement in the calculated pK_a values, together with the measured ^{1}H and ^{13}C NMR chemical-shift differences at pH = 2.4 vs. pH = 7.5, identified the imidazole imino N-atom as the most favorable protonation site. Excited-state TD-DFT calculations also achieved excellent agreement with experimentally recorded spectra and revealed that observed excitations can be classified as the π–π* transitions in all cases. Together with the calculated pK_a constants, these also ruled out the existence of deprotonated anionic species under employed conditions and suggested a partial existence of diprotonated **6-H**[++] at very low pH values.

As an extension of the current work, computational analysis predicted that system **9**, made by introducing an additional isobutylamine group on the benzimidazole unit in **6**, would have pK_a = 7.0, making it very useful for detecting changes on going from neutral to immediately acidic media in a wide range of optical sensing applications.

References

1.   Wang, B.; Anslyn, E.V. *Chemosensors: Principles, Strategies and Applications*; Wiley-VCH: Weinheim, Germany, 2011.
2.   Valeur, B.; Leray, I. Design principles of fluorescent molecular sensors for cation recognition. *Coord. Chem. Rev.* **2000**, *205*, 3–40. [CrossRef]
3.   Wu, D.; Chen, L.; Lee, W.; Ko, G.; Yin, J.; Yoon, J. Recent progress in the development of organic dye based near-infrared fluorescence probes for metal ions. *Coord. Chem. Rev.* **2018**, *354*, 74–97. [CrossRef]
4.   Wencel, D.; Abel, T.; McDonagh, C. Optical chemical pH sensors. *Anal. Chem.* **2014**, *86*, 15–29. [CrossRef] [PubMed]
5.   Bodedla, G.B.; Thomas, K.R.J.; Kumar, S.; Jou, J.H.; Li, C.J. Phenothiazine-based bipolar green-emitters containing benzimidazole units: Synthesis, photophysical and electroluminescence properties. *RSC Adv.* **2015**, *5*, 87416–87428. [CrossRef]
6.   Kim, T.D. D–π–A Conjugated molecules for optoelectronic applications. *Macromol. Rapid Commun.* **2015**, *36*, 943–958. [CrossRef] [PubMed]
7.   Debia, N.P.; Rodríguez, J.J.P.; da Silveira, C.H.; Chaves, O.A.; Iglesias, B.A.; Rodembusch, F.S.; Lüdtke, D.S. Synthesis and photophysics of benzazole based triazoles with amino acid-derived pendant units. Multiparametric optical sensors for BSA and CT-DNA in solution. *J. Mol. Liq.* **2020**, *309*, 113092. [CrossRef]
8.   Burke, C.S.; McGaughey, O.; Sabattie, J.M.; Barry, H.; McEvoy, A.K.; McDonagh, C.; MacCraith, B.D. Development of an integrated optic oxygen sensor using a novel, generic platform. *Analyst* **2005**, *130*, 41–45. [CrossRef]
9.   Horak, E.; Vianello, R.; Murković Steinberg, I. Optical sensing (nano)materials based on benzimidazole derivatives. In *Chemistry and Applications of Benzimidazole and Its Derivatives*; Marinescu, M., Ed.; IntechOpen: London, UK, 2019; pp. 184–205.
10. Pfeifer, D.; Klimant, I.; Borisov, S.M. Ultrabright red-emitting photostable perylene bisimide dyes: New indicators for ratiometric sensing of high pH or carbon dioxide. *Chem. Eur. J.* **2018**, *24*, 10711–10720. [CrossRef]
11. Silverman, R.B. *The organic Chemistry of Drug Design and Drug Action*, 2nd ed.; Elsevier Academic Press: London, UK, 2004.
12. Keri, R.S.; Hiremathad, A.; Budagumpi, S.; Nagaraja, B.M. Comprehensive review in current developments of benzimidazole-based medicinal chemistry. *Chem. Biol. Drug Des.* **2015**, *86*, 19–65. [CrossRef]
13. Akhtar, J.; Khan, A.A.; Ali, Z.; Haider, R.; Shahar Yar, M. Structure-activity relationship (SAR) study and design strategies of nitrogen-containing heterocyclic moieties for their anticancer activities. *Eur. J. Med. Chem.* **2017**, *125*, 143–189. [CrossRef]
14. Kumar, G.; Gupta, N.; Paul, K.; Luxami, V. Acrylonitrile embedded benzimidazole-anthraquinone based chromofluorescent sensor for ratiometric detection of CN− ions in bovine serum albumin. *Sens. Actuators B Chem.* **2018**, *267*, 549–558. [CrossRef]
15. Staneva, D.; Betcheva, R. Synthesis and functional properties of new optical pH sensor based on benzo[*de*]anthracen-7-one immobilized on the viscose. *Dyes Pigm.* **2007**, *74*, 148–153. [CrossRef]
16. Chen, W.; Ma, X.; Chen, H.; Liu, S.H.; Yin, J. Fluorescent probes for pH and alkali metal ions. *Coord. Chem. Rev.* **2021**, *427*, 213584. [CrossRef]
17. Steinegger, A.; Wolfbeis, O.S.; Borisov, S.M. Optical sensing and imaging of pH values: Spectroscopies, materials, and applications. *Chem. Rev.* **2020**, *120*, 12357–12489. [CrossRef] [PubMed]
18. Shamsipur, M.; Barati, A.; Nematifar, Z. Fluorescent pH nanosensors: Design strategies and applications. *J. Photochem. Photobiol. C* **2019**, *39*, 76–141. [CrossRef]
19. Nawaz, H.; Tian, W.; Zhang, J.; Jia, R.; Yang, T.; Yu, J.; Zhang, J. Visual and precise detection of pH values under extreme acidic and strong basic environments by cellulose-based superior sensor. *Anal. Chem.* **2019**, *91*, 3085–3092. [CrossRef]
20. Hranjec, M.; Horak, E.; Tireli, M.; Pavlović, G.; Karminski-Zamola, G. Synthesis, crystal structure and spectroscopic study of novel benzimidazoles and benzimidazo[1,2-*a*]quinolines as potential chemosensors for different cations. *Dyes Pigment.* **2012**, *95*, 644–656. [CrossRef]
21. Hranjec, M.; Horak, E.; Babić, D.; Plavljanin, S.; Srdović, Z.; Murković Steinberg, I.; Vianello, R.; Perin, N. Fluorescent benzimidazo[1,2-*a*]quinolines: Synthesis, spectroscopic and computationalstudies of protonation equilibria and metal ion sensitivity. *New J. Chem.* **2017**, *41*, 358–371. [CrossRef]
22. Carey, W.P.; DeGrandpre, M.D.; Jorgensen, B.S. Polymer-coated cylindrical waveguide absorption sensor for high acidities. *Anal. Chem.* **1989**, *61*, 1674–1678. [CrossRef]
23. Perin, N.; Bobanović, K.; Zlatar, I.; Jelić, D.; Kelava, V.; Koštrun, S.; Gabelica Marković, V.; Brajša, K.; Hranjec, M. Antiproliferative activity of amino substituted benzo[*b*]thieno[2,3-*b*]pyrido[1,2-*a*]benzimidazoles explored by 2D and 3D cell culture system. *Eur. J. Med. Chem.* **2017**, *125*, 722–735. [CrossRef]
24. Horak, E.; Kassal, P.; Hranjec, M.; Murković Steinberg, I. Benzimidazole functionalized Schiff bases: Novel pH sensitive fluorescence turn-on chromoionophores for ion-selective optodes. *Sens. Actuators B Chem.* **2018**, *258*, 415–423. [CrossRef]

25. Marenich, A.V.; Cramer, C.J.; Truhlar, D.G. Universal solvation model based on solute electron density and on a continuum model of the solvent defined by the bulk dielectric constant and atomic surface tensions. *J. Phys. Chem. B* **2009**, *113*, 6378–6396. [CrossRef] [PubMed]
26. Hok, L.; Vianello, R. Direct metal-free transformation of alkynes to nitriles: Computational evidence for the precise reaction mechanism. *Int. J. Mol. Sci.* **2021**, *22*, 3193. [CrossRef]
27. Rowlands, G.J.; Severinsen, R.J.; Buchanan, J.K.; Shaffer, K.J.; Jameson, H.T.; Thennakoon, N.; Leito, I.; Lõkov, M.; Kütt, A.; Vianello, R.; et al. Synthesis and basicity studies of quinoline[7,8-*h*]quinoline derivatives. *J. Org. Chem.* **2020**, *85*, 11297–11308. [CrossRef]
28. Tissandier, M.D.; Cowen, K.A.; Feng, W.Y.; Gundlach, E.; Cohen, M.H.; Earhart, A.D.; Coe, J.V.; Tuttle, T.R. The proton's absolute aqueous enthalpy and Gibbs free energy of solvation from cluster-ion solvation data. *J. Phys. Chem. A* **1998**, *102*, 7787–7794. [CrossRef]
29. Grimme, S.; Antony, J.; Ehrlich, S.; Krieg, H. A consistent and accurate ab initio parametrization of density functional dispersion correction (DFT-D) for the 94 elements H–Pu. *J. Chem. Phys.* **2010**, *132*, 154104. [CrossRef]
30. Dennington, R.; Keith, T.A.; Millam, J.M. *GaussView*, Version 6.0; Semichem Inc.: Shawnee Mission, KS, USA, 2016.
31. Frisch, M.J.; Trucks, G.W.; Schlegel, H.B.; Scuseria, G.E.; Robb, M.A.; Cheeseman, J.R.; Scalmani, G.; Barone, V.; Petersson, G.A.; Nakatsuji, H.; et al. *Gaussian 16*, Revision C.01; Gaussian, Inc.: Wallingford, CT, USA, 2016.
32. Demchenko, A.P. Introduction to fluorescence sensing. *Anal. Bioanal. Chem.* **2009**, *395*, 1195–1196.
33. Benassi, R.; Grandi, R.; Pagnoni, U.M.; Taddei, F. Study of the effect of N-protonation and N-methylation on the ^{1}H and ^{13}C chemical shifts of the six-membered ring in benzazoles and 2-substituted *N,N*-dimethylamino derivatives. *Magn. Reson. Chem.* **1986**, *24*, 415–420. [CrossRef]
34. Tshepelevitsh, S.; Kütt, A.; Lõkov, M.; Kaljurand, I.; Saame, J.; Heering, A.; Plieger, P.G.; Vianello, R.; Leito, I. On the basicity of organic bases in different media. *Eur. J. Org. Chem.* **2019**, *2019*, 6735–6748. [CrossRef]
35. Vianello, R.; Maksić, Z.B. Towards highly powerful neutral organic superacids—A DFT study of some polycyano derivatives of planar hydrocarbons. *Tetrahedron* **2005**, *61*, 9381–9390. [CrossRef]
36. Valadbeigi, Y. Design of strongest organic Broensted acids in gas phase. *Chem. Phys. Lett.* **2017**, *681*, 50–55. [CrossRef]
37. Martin, R.L. Natural transition orbitals. *J. Chem. Phys.* **2003**, *118*, 4775–4777. [CrossRef]
38. Lakowicz, J.R. *Principles of Fluorescence Spectroscopy*, 2nd ed.; Kluwer: New York, NY, USA, 1999.